



Equilibrium Spacetime Correlations of the Toda Lattice on the Hydrodynamic Scale

Guido Mazzuca¹ · Tamara Grava^{2,3,4} · Thomas Kriecherbauer⁵ · Kenneth T.-R. McLaughlin⁶ · Christian B. Mendl⁷ · Herbert Spohn⁸

Received: 18 January 2023 / Accepted: 31 July 2023 / Published online: 25 August 2023
© The Author(s) 2023

Abstract

We report on molecular dynamics simulations of spacetime correlations of the Toda lattice in thermal equilibrium. The correlations of stretch, momentum, and energy are computed numerically over a wide range of pressure and temperature. Our numerical results are compared with the predictions from linearized generalized hydrodynamics on the Euler scale. The system size is $N = 3000, 4000$ and time $t = 600$, at which ballistic scaling is well confirmed. With no adjustable parameters, the numerically obtained scaling functions agree with the theory within a precision of less than 3.5%.

Keywords Toda lattice · Integrable systems · Generalized hydrodynamics · Correlation functions

1 Introduction

A central goal of Statistical Mechanics is to explore the structure of equilibrium correlations for observables of physical interest. These could be static correlations, but more ambitiously also correlations in spacetime. For our contribution the focus is one-dimensional classical fluids with a short range interaction potential. Their static correlations have exponential decay [18, 36]. Spacetime correlations are generically concentrated in three narrow peaks. The heat peak has zero velocity and broadens in time as $t^{\frac{3}{5}}$. In addition there are the two sound peaks with velocity $\pm c, c > 0$ the isentropic speed of sound. These peaks broaden with the characteristic power law $t^{\frac{2}{3}}$ [3, 50]. Such super-diffusive spreading is a feature special for one dimension. However, known are also fine-tuned interaction potentials such that the mechanical system is integrable. The most famous one is the Calogero fluid for which the

Communicated by T. Prosen.

Tamara Grava, Thomas Kriecherbauer, Kenneth T-R McLaughlin, Christian B. Mendl and Herbert Spohn have contributed equally to this work.

✉ Guido Mazzuca
mazzuca@kth.se

Extended author information available on the last page of the article

interaction potential is $1/\sinh^2(x)$ with x denoting the distance between two particles. At low density the Calogero fluid can be approximated by the Toda chain with interaction $4e^{-2x}$ between particles having neighboring labels. The latter system will be at the center of our investigations. A further model is the hard rod fluid for which the spacetime correlator in one-particle phase space has been computed exactly [33].

Integrable models have an extensive number of conservation laws. On a very heuristic level, every conservation law adds a further spectral line travelling with its own characteristic velocity. Thus for the infinitely extended system, at least to leading order, the spacetime correlator is expected to scale ballistically and to be governed by a smooth profile. For hard rods this structure can be deduced from the exact solution. Beyond hard rods no such result is available. On the theoretical side the situation has improved dramatically through the 2016 construction of generalized hydrodynamics (GHD) [4, 7]. As noted by [12] in the context of the Lieb-Liniger δ -Bose gas, the ballistic part of the spacetime correlator can be computed from GHD linearized at thermal equilibrium. With such predictions a quantitative comparison between theory and molecular dynamics (MD) simulations is in reach.

The broad spectrum of the spacetime correlator has been observed already in pre-GHD simulations. As examples we only mention the MD simulation [42] of the Ablowitz-Ladik model, an integrable discretization of the nonlinear Schrödinger equation, and the MD simulation [30] of the Toda lattice for few parameter values. Thereby the conventional Landau-Lifshitz theory is extended from a few to a large number of modes. A further extension concerns initial states which are not spacetime stationary [9], thus not thermal equilibrium. Linearized GHD is also a powerful tool to investigate the correlations of quantum spin chains in great detail [11]. From the side of condensed matter physics, the interest is mainly focused on integrable quantum models, as the XYZ spin chain and the spin- $\frac{1}{2}$ Fermi-Hubbard model. Such models are accessible to time-dependent DMRG simulations, see [5, 6] for examples. The rigid limitations in size and number of equilibrium samples makes the simulation of correlations a challenging enterprise and often the simulation of macroscopic profiles are preferred. In recent years, particular attention has been given to the spacetime spin-spin correlation of the XXZ model at half-filling and at the isotropic point [13, 27, 34]. The same quantity has also been investigated for a discrete classical chain with 3-spins of unit length and interactions such that the model is integrable [8]. A comparable situation occurs for the classical sinh-Gordon equation, which is integrable as a nonlinear continuum wave equation and possesses an integrable discretization, see [2] for MD simulations for equilibrium time correlations of the discrete model.

For a specific model under study, linearized GHD requires the knowledge of the two-particle scattering shift, the density of states of the equilibrium Lax matrix, the static correlator, and the effective velocity of the modes. While the first item is known analytically for all models, for the other items one has to solve numerically the TBA equation and the linear integral equation determining the effective velocity. These tasks can be accomplished with modest numerical efforts. The real challenge are MD simulations of the deterministic dynamics for sufficiently large system size and with a huge number of samples so to reduce the unavoidable noise. For the Toda lattice these conditions can be met and we arrive at a *parameter free* comparison between MD and linearized GHD.

To provide a brief outline, in the following section we recall the Landau-Lifshitz theory for the nonintegrable case of three conservation laws. With this input the extension to the integrable Toda lattice can be grasped more easily. In Sect. 4 we report on our MD simulations, estimate the noise level of data, and compare with the predictions from linearized GHD. The Toda lattice is simulated with periodic boundary conditions. Thus, the available time span of

simulation is linearly linked to system size. In particular, with our methods we cannot study the long time behavior beyond the Euler scale.

2 Landau–Lifshitz Theory

The dynamics of the Toda chain is governed by the hamiltonian

$$H = \sum_{j \in \mathbb{Z}} \left(\frac{1}{2} p_j^2 + \exp(-(q_{j+1} - q_j)) \right), \tag{1}$$

where $(q_j, p_j) \in \mathbb{R}^2$ are position and momentum of the j -th particle [54, 55]. Introducing the j -th stretch (free volume) through $r_j = q_{j+1} - q_j$, the equations of motion read

$$\frac{d}{dt} r_j = p_{j+1} - p_j, \quad \frac{d}{dt} p_j = -e^{-r_j} + e^{-r_{j-1}}, \quad j \in \mathbb{Z}. \tag{2}$$

By tradition, one introduces coefficients for the range and strength of the interaction potential through $(g/\gamma) \exp(-\gamma(q_{j+1} - q_j))$. However, by a suitable change of spacetime scales, the form (2) can be regained, see the discussion in Sect. 5. The Toda hamiltonian has no free parameters. Since the equilibrium measure for (1) is of product form, static correlations are easily accessible. Time correlations are more challenging, see [46, 47] for early attempts. A novel approach relies on GHD. The guiding idea is to first identify the hydrodynamic conservation laws. Given such an input one can construct the corresponding Landau-Lifshitz theory [17, 32], as based on linearized GHD.

Before entering into details, it will be useful to first recall the Landau-Lifshitz theory for a chain with a generic interaction potential, denoted by V (for the Toda lattice $V(x) = e^{-x}$), see [50] and references listed therein. Thus in (1) the interaction term reads $V(q_{j+1} - q_j)$ and the equations of motion become

$$\frac{d}{dt} r_j = p_{j+1} - p_j, \quad \frac{d}{dt} p_j = V'(r_j) - V'(r_{j-1}). \tag{3}$$

To define spacetime correlations we first have to specify the random initial data modelling thermal equilibrium. By Galileian invariance one restricts to the case of zero average momentum. Then the Gibbs states are characterized by the inverse temperature $\beta > 0$ and a parameter P such that the physical pressure equals P/β . For simplicity, we will refer to P also as pressure. The allowed range of P depends on V . If V diverges faster than $|x|$ for $|x| \rightarrow \infty$, then $P \in \mathbb{R}$. For the Toda lattice $P > 0$ because of the one-sided divergence of the exponential. In thermal equilibrium $\{(r_j, p_j), j \in \mathbb{Z}\}$ are a collection of i.i.d. random variables with single site probability density

$$Z_0(P, \beta)^{-1} \exp\left(-\beta \left(\frac{1}{2} p_0^2 + V(r_0)\right) - P r_0\right). \tag{4}$$

Here $Z_0(P, \beta)$ is the normalizing partition function. Note that, with our convention, P and β appear linearly in the exponent. Expectations with respect to such i.i.d. random variables are denoted by $\langle \cdot \rangle_{P, \beta}$. We also shorten the notation for the covariance through $\langle X_1 X_2 \rangle_{P, \beta}^c = \langle X_1 X_2 \rangle_{P, \beta} - \langle X_1 \rangle_{P, \beta} \langle X_2 \rangle_{P, \beta}$, where the particular random variables X_1, X_2 will be obvious from the context.

For general V , the conserved fields are stretch, momentum, and energy with densities

$$\mathbf{Q}(j) = (r_j, p_j, e_j), \quad e_j = \frac{1}{2}p_j^2 + V_j, \tag{5}$$

using as shorthand $V_j = V(r_j)$. \mathbf{Q} is a three-vector with components labeled by $n = 0, 1, 2$. The static space correlator is defined through

$$C_{m,n}(j) = \langle Q_m(j) Q_n(0) \rangle_{P,\beta}^c \tag{6}$$

and the static susceptibility by summing over space,

$$C_{m,n} = \sum_{j \in \mathbb{Z}} \langle Q_m(j) Q_n(0) \rangle_{P,\beta}^c, \tag{7}$$

$m, n = 0, 1, 2$. Since the underlying measure is product, only the $j = 0$ term is nonvanishing and

$$C = \begin{pmatrix} \langle r_0 r_0 \rangle_{P,\beta}^c & 0 & \langle r_0 e_0 \rangle_{P,\beta}^c \\ [0.5ex] 0 & \langle p_0 p_0 \rangle_{P,\beta}^c & 0 \\ [0.5ex] \langle r_0 e_0 \rangle_{P,\beta}^c & 0 & \langle e_0 e_0 \rangle_{P,\beta}^c \end{pmatrix}, \tag{8}$$

the zero entries resulting from $\langle p_0 \rangle_{P,\beta} = 0$, $\langle p_0^3 \rangle_{P,\beta} = 0$, and r_0, p_0 being independent random variables. Later on we will need the statistical properties of the conserved fields on the hydrodynamic scale. More precisely, for smooth test functions f , we consider the random field

$$\xi_\epsilon(f) = \sqrt{\epsilon} \sum_{j \in \mathbb{Z}} f(\epsilon j) (\mathbf{Q}(j) - \langle \mathbf{Q}(0) \rangle_{P,\beta}). \tag{9}$$

Then, by the central limit theorem for independent random variables,

$$\lim_{\epsilon \rightarrow 0} \xi_\epsilon(f) = \int_{\mathbb{R}} dx f(x) \mathbf{u}(x), \tag{10}$$

where the limit field $\mathbf{u}(x)$ is a Gaussian random field on \mathbb{R} with mean zero, $\mathbb{E}(\mathbf{u}(x)) = 0$, and covariance

$$\mathbb{E}(u_m(x) u_n(x')) = C_{m,n} \delta(x - x'), \tag{11}$$

in other words, $\mathbf{u}(x)$ is Gaussian white noise with correlated components.

Microscopically, spacetime correlations are defined by evolving one of the observables to time t which yields

$$S_{m,n}(j, t) = \langle Q_m(j, t) Q_n(0, 0) \rangle_{P,\beta}^c. \tag{12}$$

Note that the Gibbs measure is spacetime stationary and thus without loss of generality both arguments in Q_n in (12) can be taken as $(0, 0)$. To understand the structure of $S_{m,n}$ one has to rely on approximations. For the long time ballistic regime a standard scheme is the Landau-Lifshitz theory, which views $Q_n(0, 0)$ as a small perturbation of the initial Gibbs measure at the origin. This perturbation will propagate and is then probed by the average of Q_m at the spacetime point (j, t) . For large (j, t) the microscopic dynamics is approximated by the Euler equations, but only in their linearized version since the perturbation is small. More concretely, the approximate theory will be a continuum field $\mathbf{u}(x, t)$ over $\mathbb{R} \times \mathbb{R}$, which is governed by

$$\partial_t \mathbf{u}(x, t) + \mathbf{A} \partial_x \mathbf{u}(x, t) = 0, \tag{13}$$

with random initial conditions as specified in (11). The 3×3 flux Jacobian \mathbf{A} is constant, i.e. independent of (x, t) . To explain the structure of \mathbf{A} requires some further efforts. We refer to [50] for more details and proofs of the key identities.

From the equations of motion one infers that to each density $Q_n(j, t)$ there is a current density $J_n(j, t)$ such that

$$\frac{d}{dt} Q_n(j, t) + J_n(j, t) - J_n(j - 1, t) = 0. \tag{14}$$

Explicitly, the current densities are

$$\mathbf{J}(j) = -(p_j, V'_{j-1}, p_j V'_{j-1}), \tag{15}$$

where we adopted the convention that omission of time argument t means time 0 fields. One then defines the static current-conserved field correlator

$$B_{m,n}(j) = \langle J_m(j) Q_n(0) \rangle_{P,\beta}^c, \tag{16}$$

and the corresponding susceptibility

$$B_{m,n} = \sum_{j \in \mathbb{Z}} \langle J_m(j) Q_n(0) \rangle_{P,\beta}^c. \tag{17}$$

Despite its asymmetric looking definition,

$$B_{m,n} = B_{n,m}. \tag{18}$$

As a general property, Euler equations are built on thermally averaged currents. Linearizing them with respect to the average fields yields

$$A = BC^{-1}. \tag{19}$$

Here B appears when differentiating the average currents with respect to the chemical potentials and C^{-1} when switching from intensive to extensive variables. By construction $C = C^T$ and $C > 0$, in addition $B = B^T$ according to (18). Hence

$$A = C^{1/2} C^{-1/2} B C^{-1/2} C^{-1/2}, \tag{20}$$

which ensures that A has real eigenvalues and a complete set of left-right eigenvectors. Anharmonic lattices are symmetric under time reversal, which implies the eigenvalues $\mathbf{c} = (-c, 0, c)$, with $c > 0$ the isentropic speed of sound. We denote the right, resp. left eigenvectors of A by $|\psi_\alpha\rangle$ and $\langle \tilde{\psi}_\alpha|$, $\alpha = 0, 1, 2$. With this input the solution to (13) with initial conditions (11) reads

$$\begin{aligned} S_{m,n}^{LL}(x, t) &= \mathbb{E}(u_m(x, t) u_n(0, 0)) \\ &= (\delta(x - At) \mathbf{C})_{m,n} = \sum_{\alpha=0}^2 \delta(x - c_\alpha t) (|\psi_\alpha\rangle \langle \tilde{\psi}_\alpha| \mathbf{C})_{m,n} \end{aligned} \tag{21}$$

with $m, n = 0, 1, 2$. There are three δ -peaks, the heat peak standing still and two sound peaks propagating in opposite directions with speed c . Specifying m, n , each peak has a signed weight which depends on C and the left-right eigenvectors of A .

The Landau-Lifshitz theory asserts that the microscopic correlator

$$S_{m,n}(j, t) \simeq S_{m,n}^{LL}(x, t) \tag{22}$$

for $j = \lfloor xt \rfloor$, $\lfloor \cdot \rfloor$ denoting integer part, with t sufficiently large. The reader might be disappointed by the conclusion. But with such basic information the fine-structure of the peaks can be investigated, in particular their specific sub-ballistic broadening and corresponding scaling functions [41, 49, 50].

When turning to the Toda lattice, the conservation laws are now labeled by $n = 0, 1, \dots$ and thus A, B, C become infinite dimensional matrices. The corresponding Landau-Lifshitz theory has been worked out in [51] using the recipe from above: the matrices B and C are computed exactly on the basis of thermal GGE. The matrix A is still defined through (19). However the expression (22) holds approximately only in the ballistic regime.

3 Toda Lattice, Linearized Generalized Hydrodynamics

The conservation laws of the Toda lattice are obtained from a Lax matrix [15, 35]. For this purpose, we first introduce the Flaschka variables

$$a_j = e^{-r_j/2}. \tag{23}$$

Then the equations of motion become

$$\frac{d}{dt} a_j = \frac{1}{2} a_j (p_j - p_{j+1}), \quad \frac{d}{dt} p_j = a_{j-1}^2 - a_j^2. \tag{24}$$

The Lax matrix, L , is defined by

$$L_{j,j} = p_j, \quad L_{j,j+1} = L_{j+1,j} = a_j, \tag{25}$$

$j \in \mathbb{Z}$, and $L_{i,j} = 0$ otherwise. Clearly $L = L^T$. The conserved fields are labelled by nonnegative integers and have densities given by

$$Q_0(j) = \frac{1}{2}(r_{j-1} + r_j), \quad Q_n(j) = (L^n)_{j,j}, \tag{26}$$

with $n \geq 1$. Note that $Q_n(j)$ is local in the sense that it depends only on the variables with indices in the interval $[j - n, j + n]$. An explicit expression for these quantities is given in [20]. For the current densities one obtains

$$J_0(j) = -\frac{1}{2}(p_{j+1} + p_j), \quad J_n(j) = (L^n L^\downarrow)_{j,j}, \quad n = 1, 2, \dots, \tag{27}$$

where L^\downarrow is the lower triangular part of L . Then under the Toda dynamics

$$\frac{d}{dt} Q_n(j, t) + J_n(j, t) - J_n(j - 1, t) = 0, \tag{28}$$

which is the n -th conservation law in local form.

The conserved field $n = 1$ is momentum and agrees with the definition in (5). For the stretch we use a variant which is reflection symmetric relative to the origin. For $n = 2$ one obtains $(L^2)_{0,0} = p_0^2 + a_{-1}^2 + a_0^2$ and $(L^2 L^\downarrow)_{0,0} = a_0^2(p_0 + p_1)$ which differs from (5) and (15) by the trivial factor of 2. In our numerical plots we use the physical energy density e_j . However we touched upon a more subtle issue. Densities are not uniquely defined, since one can add a difference of some local function and its shift by one. When summing a particular choice for the density over some spatial interval, the result differs from another choice of the density by a boundary term only. Thus the bulk term will have a correction of order $1/(\text{length of interval})$, which does not affect the hydrodynamic equations. For the currents the difference can be written as a total time derivative which is again a boundary term when integrating over some time interval. In this section we adopt the conventions (26) and (27), since the analysis heavily relies on the Lax matrix. Beyond $n = 2$, while the fields no longer have a name, they still have to be taken into account in a hydrodynamic theory.

The infinite volume static field-field correlator is defined as in (6) and the current-field correlator as in (16). In particular, $B = B^T$. Of course, C, B are now matrices in the Hilbert space of sequences indexed by \mathbb{N}_0 , i.e. the space $\ell_2(\mathbb{N}_0)$. To distinguish 3×3 matrices from their infinite dimensional counterparts, for the latter we use standard italic symbols. The spacetime correlator of the Toda lattice is defined by

$$S_{m,n}(j, t) = \langle Q_m(j, t) Q_n(0, 0) \rangle_{P,\beta}^c. \tag{29}$$

Using invariance under space reversal of the dynamics and the equilibrium covariance matrix, the correlator satisfies the symmetry

$$S_{m,n}(j, t) = (-1)^{m+n} S_{m,n}(-j, t) \tag{30}$$

for $m, n = 0, 1, 2$, for details see [48], Chapter 15. Adding time reversal symmetry, in general one concludes

$$S_{m,n}(j, t) = S_{m,n}(-j, -t). \tag{31}$$

As a first step, the free energy of the Toda lattice is given by

$$F_{\text{eq}}(P, \beta) = \log \sqrt{\beta/2\pi} + P \log \beta - \log \Gamma(P). \tag{32}$$

In particular, the average stretch, ν , is determined through

$$\nu(P, \beta) = \partial_P F_{\text{eq}}(P, \beta) = \langle Q_0(0) \rangle_{P,\beta} = \log \beta - \psi(P), \tag{33}$$

with ψ the digamma function. Expectations of higher order fields can be written as moments of a probability measure denoted by $\nu\rho_p$,

$$\kappa_n = \langle Q_n(0) \rangle_{P,\beta} = \int_{\mathbb{R}} dw \nu\rho_p(w) w^n, \tag{34}$$

$n \geq 1$. ρ_p is called particle density. To determine this density one first has to solve the thermodynamic Bethe equations (TBA). For this purpose we introduce the integral operator

$$Tf(w) = 2 \int_{\mathbb{R}} dw' \log |w - w'| f(w'), \tag{35}$$

$w \in \mathbb{R}$, considered as an operator on $L^2(\mathbb{R}, dw)$ and define the number density

$$\rho_n(w) = e^{-\varepsilon(w)}, \tag{36}$$

with quasi-energies ε . The quasi-energies satisfy the TBA equation

$$\varepsilon(w) = \frac{1}{2} \beta w^2 - \mu - (T e^{-\varepsilon})(w), \tag{37}$$

where the chemical potential μ has to be adjusted such that

$$\int_{\mathbb{R}} dw \rho_n(w) = P. \tag{38}$$

Thereby the number density depends on the parameters P and β .

In practice, the TBA equation has to be solved numerically. But for thermal equilibrium an exact solution is available [1, 16, 45]. Denoting the solution of (37) for $\beta = 1$ and the constraint (38) by ρ_n^* one has

$$\rho_n^*(w) = \frac{e^{-w^2/2}}{\sqrt{2\pi} |\hat{f}_P(w)|^2}, \quad \hat{f}_P(w) = \int_0^\infty dt f_P(t) e^{iwt}, \quad f_P(t) = \sqrt{2\pi}^{-1} \Gamma(P)^{-1/2} t^{P-1} e^{-\frac{1}{2}t^2}. \tag{39}$$

In our numerical simulations it is of advantage to use the exact solution.

The TBA equation is a standard tool from GHD as one way to write the Euler-Lagrange equations for the variational principle associated with the generalized free energy. For the Toda lattice such a variational formula was obtained in [10, 52]. Proofs using methods from the theory of large deviations and transfer operator method have also become available [19, 23, 38, 40]. The next steps are outlined only briefly, with more details provided in [52] and [48], Chapter 7. The main goal is to explain the required numerical task on the level of linearized GHD.

We introduce the dressing transformation of some function f by

$$f^{\text{dr}} = (1 - T\rho_n)^{-1} f \tag{40}$$

with ρ_n regarded as a multiplication operator. Then number and particle density are related as

$$\rho_n(w) = \frac{\rho_p(w)}{1 + T\rho_p(w)} \tag{41}$$

with inverse

$$\rho_p = (1 - \rho_n T)^{-1} \rho_n = \rho_n \zeta_0^{\text{dr}}, \tag{42}$$

using the convention $\zeta_n(w) = w^n$.

For the average currents similar identities are available. The central novel quantity is the effective velocity

$$v^{\text{eff}} = \frac{\zeta_1^{\text{dr}}}{\zeta_0^{\text{dr}}}, \tag{43}$$

see [4, 7, 53, 56]. Then

$$\langle J_0(0) \rangle_{P,\beta} = -\kappa_1, \tag{44}$$

and, for $n \geq 1$,

$$\langle J_n(0) \rangle_{P,\beta} = \int_{\mathbb{R}} dw \rho_p(w) (v^{\text{eff}}(w) - \kappa_1) w^n. \tag{45}$$

In thermal equilibrium we have $\kappa_1 = 0$.

Since in the following there will be many integrals over \mathbb{R} , let us first introduce the abbreviation

$$\langle f \rangle = \int_{\mathbb{R}} dw f(w). \tag{46}$$

With this notation the C matrix turns out to be of the form

$$\begin{aligned} C_{0,0} &= v^3 \langle \rho_p \zeta_0^{\text{dr}} \zeta_0^{\text{dr}} \rangle, \\ C_{0,n} &= C_{n,0} = -v^2 \langle \rho_p \zeta_0^{\text{dr}} (\zeta_n - \kappa_n \zeta_0)^{\text{dr}} \rangle, \\ C_{m,n} &= v \langle \rho_p (\zeta_m - \kappa_m \zeta_0)^{\text{dr}} (\zeta_n - \kappa_n \zeta_0)^{\text{dr}} \rangle, \end{aligned} \tag{47}$$

$m, n \geq 1$. Note that the matrix C has the block structure

$$C = \begin{pmatrix} C_{0,0} & C_{0,n} \\ C_{m,0} & C_{m,n} \end{pmatrix}, \tag{48}$$

in the sense that $C_{m,n}$ for $m, n \geq 1$ follows a simple pattern. This structure will reappear for B and $e^{At} C$.

The field-current correlator B can be computed in a similar fashion with the result

$$B_{0,0} = v^2 \langle \rho_p (v^{\text{eff}} - \kappa_1) \zeta_0^{\text{dr}} \zeta_0^{\text{dr}} \rangle,$$

$$\begin{aligned}
 B_{0,n} &= B_{n,0} = -v \langle \rho_p (v^{\text{eff}} - \kappa_1) \zeta_0^{\text{dr}} (\zeta_n - \kappa_n \zeta_0)^{\text{dr}} \rangle, \\
 B_{m,n} &= \langle \rho_p (v^{\text{eff}} - \kappa_1) (\zeta_m - \kappa_m \zeta_0)^{\text{dr}} (\zeta_n - \kappa_n \zeta_0)^{\text{dr}} \rangle.
 \end{aligned}
 \tag{49}$$

As in (21), we want to determine the propagator of the Landau-Lifshitz theory, denoted by $S_{m,n}^{\text{LL}}(x, t)$. In principle, all pieces have been assembled. However to figure out the exponential of A requires its diagonalization. We only mention that one constructs a linear similarity transformation, R , such that $R^{-1}AR$ is multiplication by

$$v^{-1}(v^{\text{eff}}(w) - \kappa_1) \tag{50}$$

in $L^2(\mathbb{R}, dw)$. Here v^{eff} is the effective velocity defined in (43). Using the block convention as in (48), the spacetime correlator in the Landau-Lifshitz approximation is given by

$$\begin{aligned}
 S^{\text{LL}}(x, t) &= \int_{\mathbb{R}} dw \delta(x - tv^{-1}(v^{\text{eff}}(w) - \kappa_1)) v \rho_p(w) \\
 &\times \begin{pmatrix} v^2 \zeta_0^{\text{dr}}(w)^2 & v \zeta_0^{\text{dr}}(w) (\zeta_n - \kappa_n \zeta_0)^{\text{dr}}(w) \\ v \zeta_0^{\text{dr}}(w) (\zeta_m - \kappa_m \zeta_0)^{\text{dr}}(w) & (\zeta_m - \kappa_m \zeta_0)^{\text{dr}}(w) (\zeta_n - \kappa_n \zeta_0)^{\text{dr}}(w) \end{pmatrix}.
 \end{aligned}
 \tag{51}$$

Note that $S^{\text{LL}}(x, 0) = \delta(x)C$. As a property of the Euler equations, the expression (51) possesses exact ballistic scaling,

$$S_{m,n}^{\text{LL}}(x, t) = \frac{1}{t} S_{m,n}^{\text{LL}}(x/t, 1). \tag{52}$$

The correlator $S_{m,n}(j, t)$ is computed in our MD simulations which will then be compared with $S_{m,n}^{\text{LL}}(x, t)$. To recall, the matrices B, C are exact while the exponential of $A = BC^{-1}$ holds only on the ballistic scale.

4 Numerical Simulations

For a molecular dynamics simulation one has to first specify a finite ring $[1, \dots, N]$ with suitable boundary conditions. For the dynamics of positions q_j and momenta p_j one imposes

$$q_{N+1} = q_1 + \nu N. \tag{53}$$

The parameter ν fixes the free volume per particle and can have either sign. In our simulation, we actually allow for a fluctuating free volume by choosing random initial conditions such that $\{r_1, p_1, \dots, r_N, p_N\}$ are i.i.d. random variables with a single site distribution as specified in (4). Then the deterministic time evolution is governed by (24) with boundary conditions

$$r_0 = r_N, \quad p_{N+1} = p_1. \tag{54}$$

In fact, the boundary condition in (53) amounts to the micro-canonical constraint

$$\sum_{j=1}^N r_j = \nu N. \tag{55}$$

If one sets $\nu = \langle Q_0(0) \rangle_{P,\beta}$, then for large N , by the equivalence of ensembles, the two schemes for sampling the correlator $S_{m,n}(j, t)$ should differ by the size of statistical fluctuations. For a few representative examples we checked that indeed the equivalence of ensembles holds for the particular observables under study.

Returning to the choice of system size there is an important physical constraint. In all simulations one observes a sharp right and left front, which travel with constant speed and beyond which spatial correlations are exponentially small. On a ring necessarily the two fronts will collide after some time. Such an encounter has a noticeable effect on the molecular dynamics which is not captured by the linearized GHD analysis. Therefore the simulation time is limited by the time of first collision. Indeed, we note in Figs. 1-3 that both linearized GHD and MD clearly display maximal speeds of at most $\Delta j / \Delta t = 2$ for the entire range of (P, β, m, n) displayed in these figures. Taking into account that the initial correlations are proportional to δ_{0j} , we conclude that for a ring of size $N = 3000$ there will be no collision of the two fronts up to time $t = 750$ which is larger than $t = 600$ used in our simulations.

Before displaying and discussing our results, we provide more details on numerically solving the TBA equations and on the actual scheme used for MD.

4.1 Details of the Numerical Implementation

4.1.1 Solving Linearized GHD

To numerically solve the linearized GHD equations, we use a numerical method similar to the one from [43]. First, Eq. (39) can be expressed in terms of the parabolic cylinder function $D_\nu(z)$, which is readily available in `Mathematica`. This provides the solution to the TBA equations (37), (38).

Then, we use a simple finite element discretization of the w -dependent functions by hat functions, resulting in piecewise linear functions on a uniform grid. After precomputing the integral operator T in (36) for such hat functions, the dressing transformation (41) becomes a linear system of equations, which can be solved numerically. This procedure yields ζ_n^{dr} , and subsequently ρ_p via (42) and v^{eff} via (43). The moments can be computed from $\kappa_n = \int_{\mathbb{R}} dw v \rho_n(w) \zeta_n^{\text{dr}}(w)$, or (equivalently) Eq. (34).

To evaluate the correlator in (51), we note that the delta-function in the integrand results in a parametrized curve, with the first coordinate (corresponding to x/t) equal to \tilde{v}^{eff} from (50), and the second coordinate equal to the remaining terms in the integrand divided by the Jacobi factor $|\frac{d}{dw} \tilde{v}^{\text{eff}}(w)|$ resulting from the delta-function.

4.1.2 Molecular Dynamics Simulations

We approximate the expectation value that is contained in the MD-definition of the correlations $S_{m,n}$ in equation (29) by the following numerical scheme, whose implementation program is written in `Python`, and can be found at [37]. First, we generate the random initial conditions distributed according to the Gibbs measure, as given by (4) for the i.i.d. random variables $(r_j, p_j)_{1 \leq j \leq N}$. Specifically, the variables p_j are distributed according to a standard normal random variable, that we generate with `Numpy v1.23's` native function `random.default_rng().normal` [25], times $1/\sqrt{\beta}$. It takes a brief calculation to see that r_j can be chosen to be $-\ln(X/(2\beta))$ where X is chi-square distributed with shape parameter $2P$. We obtain the random variable X using `Numpy v1.23's` native function `random.default_rng().chisquare`. Having chosen the initial conditions in such a manner, we solve equation (2).

For the evolution, we adapt the classical Störmer–Verlet algorithm [24] of order 2 to work with the variables (\mathbf{p}, \mathbf{r}) .

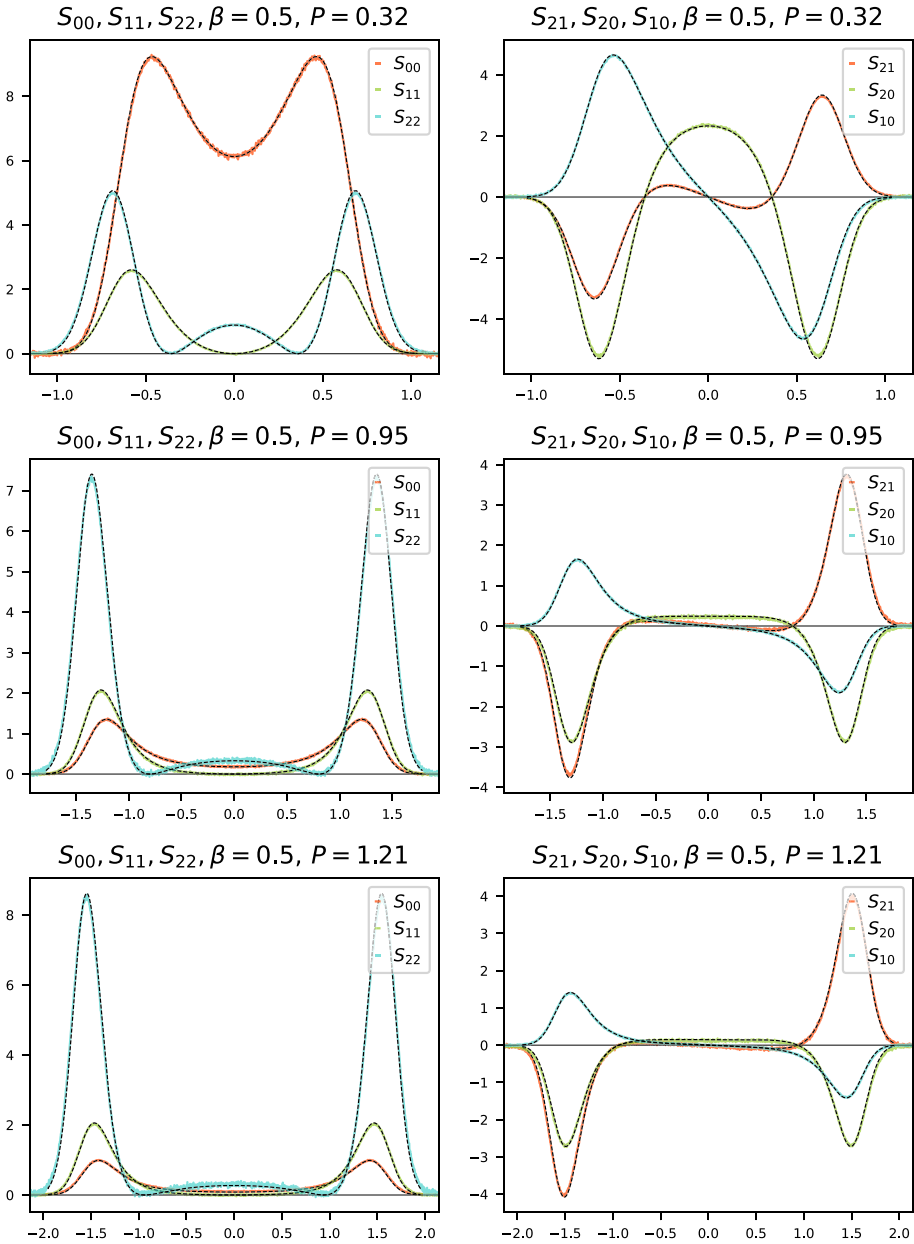


Fig. 1 Toda correlation functions: GHD predictions $y \mapsto S_{m,n}^{LL}(y, 1)$ vs. numerical simulations of the molecular dynamics $y \mapsto tS_{m,n}(yt, t)$ at $t = 600$ for $\beta = 0.5$ with low pressure (top), medium pressure (middle) and high pressure (bottom). Numerical simulations are colored according to the legend, the corresponding GHD predictions are displayed by dashed lines. Number of trials: 3×10^6

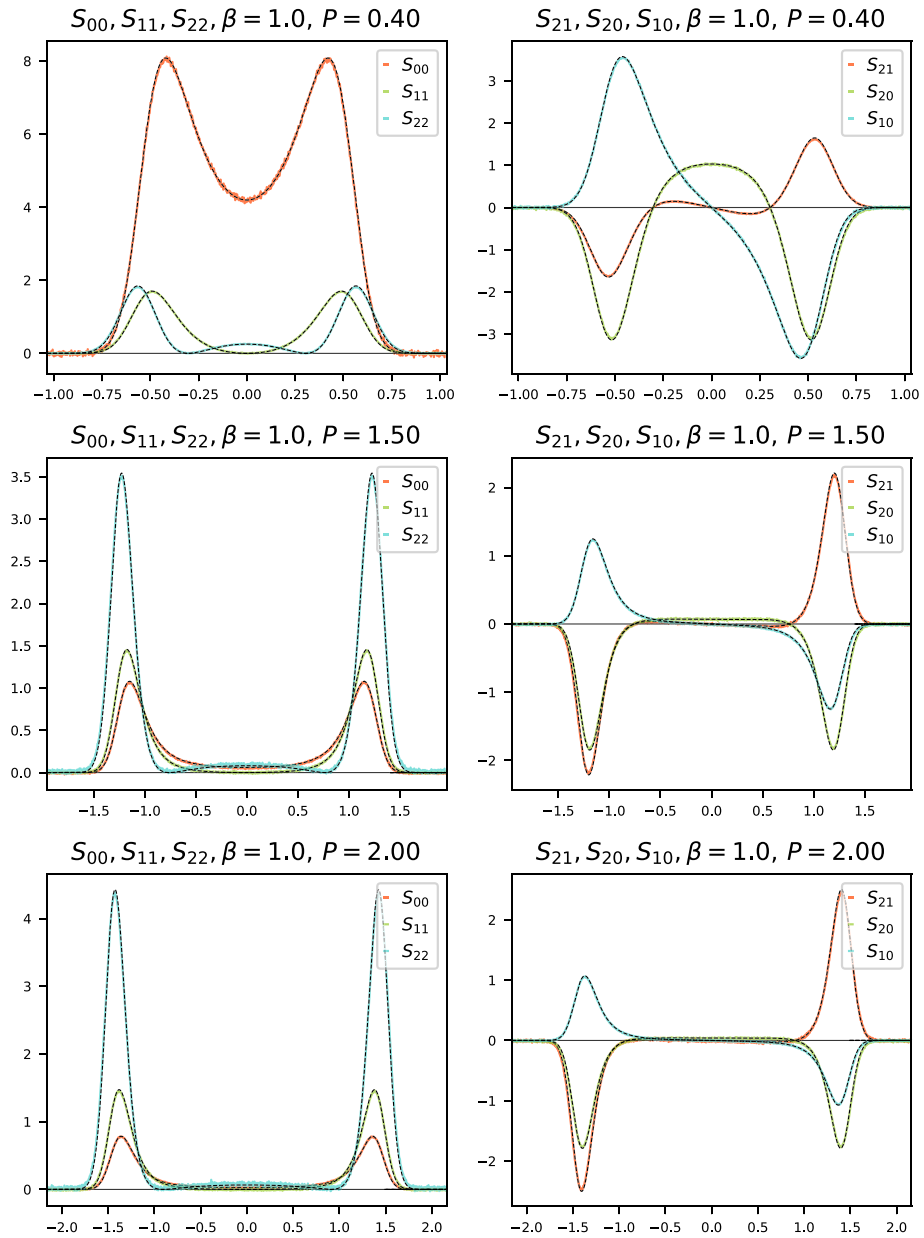


Fig. 2 Toda correlation functions: GHD predictions $y \mapsto S_{m,n}^{LL}(y, 1)$ vs. numerical simulations of the molecular dynamics $y \mapsto t S_{m,n}(yt, t)$ at $t = 600$ for $\beta = 1.0$ with low pressure (top), medium pressure (middle) and high pressure (bottom). Numerical simulations are colored according to the legend, the corresponding GHD predictions are displayed by dashed lines. Number of trials: 3×10^6

Table 1 Values for β and P and the corresponding mean stretches used in experiments

pressure	$\beta = 0.5$	$\beta = 1$	$\beta = 2$
low	$P = 0.32, \langle r \rangle \approx +2.58$	$P = 0.4, \langle r \rangle \approx +2.56$	$P = 0.52, \langle r \rangle \approx +2.56$
medium	$P = 0.95, \langle r \rangle \approx -0.03$	$P = 1.5, \langle r \rangle \approx -0.04$	$P = 2.55, \langle r \rangle \approx -0.03$
high	$P = 1.21, \langle r \rangle \approx -0.42$	$P = 2.0, \langle r \rangle \approx -0.42$	$P = 3.53, \langle r \rangle \approx -0.42$

Specifically, we used a time step equal to $\delta = 0.05$, and, given the solution $(\mathbf{r}(t), \mathbf{p}(t))$ at time t , we approximate the solution at time $t + \delta$ through the following scheme,

$$p_j \left(t + \frac{\delta}{2} \right) = p_j(t) - \frac{\delta}{2} \left(e^{-r_j(t)} - e^{r_{j-1}(t)} \right), \tag{56}$$

$$r_j(t + \delta) = r_j(t) + \delta \left(p_{j+1} \left(t + \frac{\delta}{2} \right) - p_j \left(t + \frac{\delta}{2} \right) \right), \tag{57}$$

$$p_j(t + \delta) = p_j \left(t + \frac{\delta}{2} \right) - \frac{\delta}{2} \left(e^{-r_j(t+\delta)} - e^{r_{j-1}(t+\delta)} \right), \tag{58}$$

for all $j = 1, \dots, N$. In this part of the implementation, we extensively used the library Numba [31] to speed up the computations.

Our approximation for the expectation $S_{m,n}$ is then extracted from 3×10^6 trials with independent initial conditions. Here we take the empirical mean of all trials where for each trial we also take the mean of the $N = 3000$ sets of data that are generated by choosing each site on the ring for $j = 0$.

To evaluate the quality of our numerical simulations, we have repeated the numerical experiments up to five times including variations for the length of the ring and evaluating the solutions at more intermediate time steps than displayed in the figures below. Furthermore, we have compared the results with the corresponding outcomes obtained by a MATLAB program that has been developed independently from the Python program, and that follows a different numerical scheme. It uses MATLAB’s random number generators `randn` for initial momenta and `rand` combined with the rejection method to produce initial stretches. The dynamics is then evaluated by the solver `ode45`, which exploits the Runge–Kutta method to numerically solve the Hamiltonian system associated with (1) on the ring. We found that the deviations between different experiments are comparable to the size of the amplitudes of the high frequency oscillations that are present in figures 4-5. These oscillations are due to the random fluctuations of the empirical means around their expectation values $S_{m,n}$. Agreement of different experiments up to the order of these oscillations therefore shows the consistency of the corresponding numerical results.

We also want to mention that all the pictures that appeared in this paper are made using the library `matplotlib` [26].

4.2 Comparison of Linearized GHD with MD at Time $t = 600$

We compare the GHD predictions with MD simulations for three different temperatures that correspond to $\beta = 0.5$ (Fig. 1), $\beta = 1$ (Fig. 2), and $\beta = 2$ (Fig. 3). For each β we choose three different values for the pressure parameter P in such a way that the corresponding mean stretches, given by (33), are positive (≈ 2.57) for low pressure, negative (≈ -0.42) for high pressure and approximately zero for medium pressure. We summarize their values in Table 1.

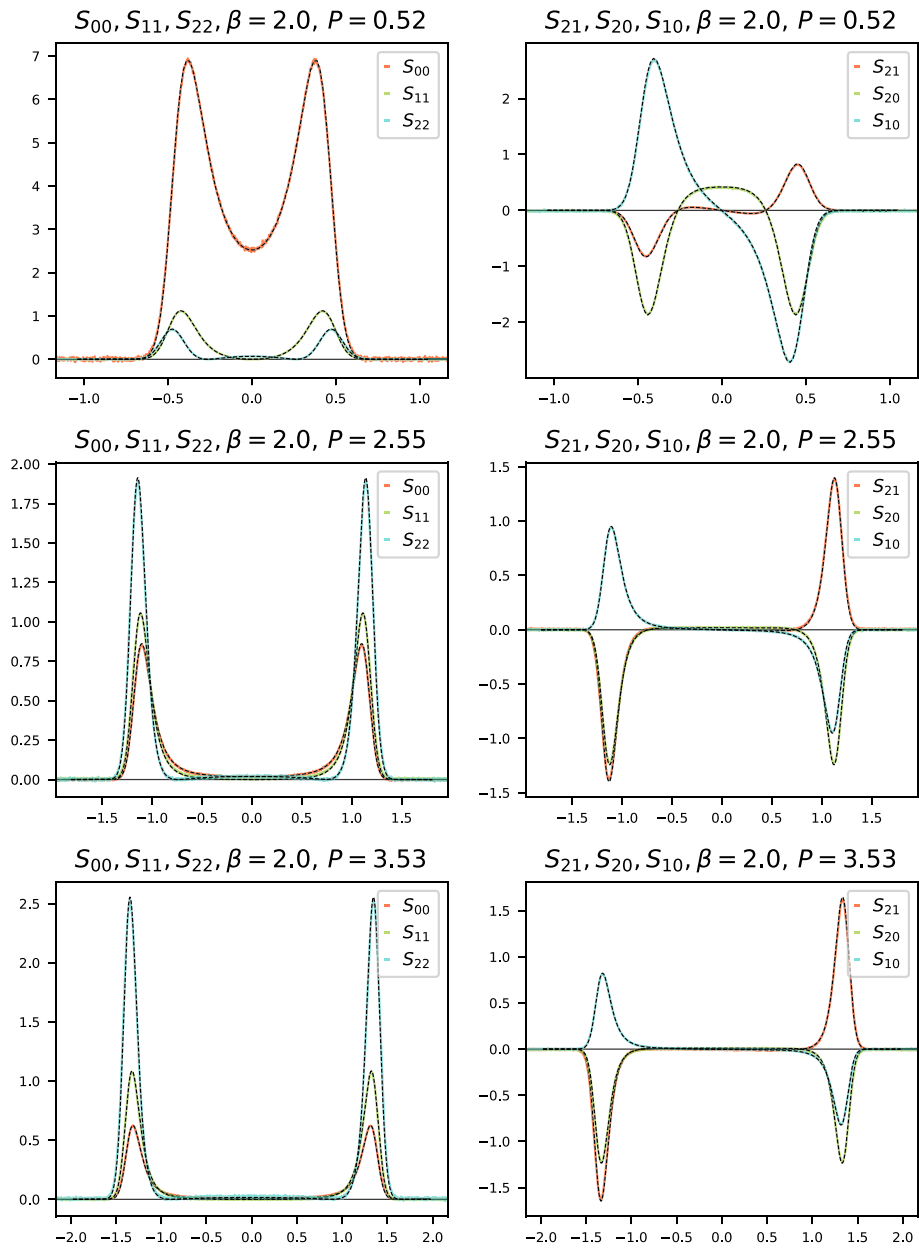


Fig. 3 Toda correlation functions: GHD predictions $y \mapsto S_{m,n}^{LL}(y, 1)$ vs. numerical simulations of the molecular dynamics $y \mapsto tS_{m,n}(yt, t)$ at $t = 600$ for $\beta = 2.0$ with low pressure (top), medium pressure (middle) and high pressure (bottom). Numerical simulations are colored according to the legend, the corresponding GHD predictions are displayed by dashed lines. Number of trials: 3×10^6

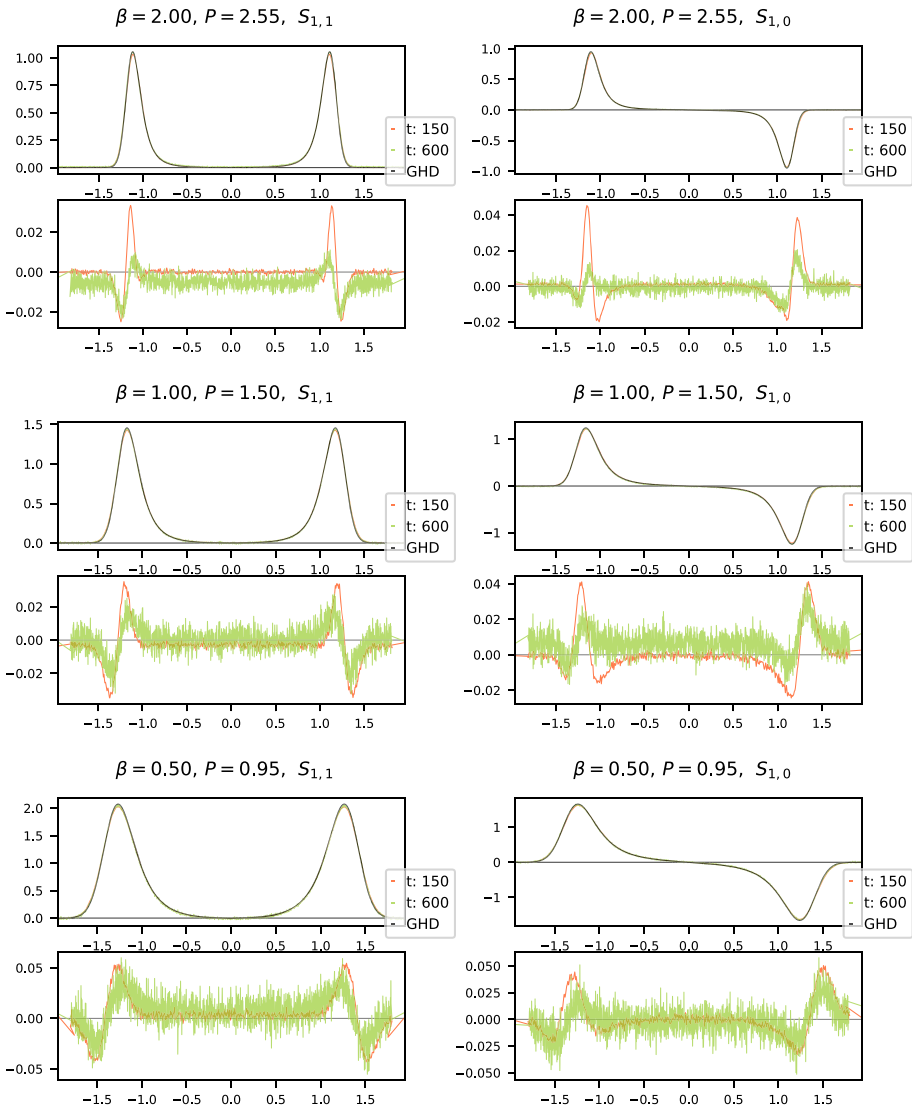


Fig. 4 Toda correlation functions $S_{1,1}$ (left) and $S_{1,0}$ (right) for medium pressure and increasing temperatures (top to bottom). For each value of β and P the top panels show GHD prediction vs. numerical simulations as in Figs. 1-3 but with the the molecular dynamics evaluated at two times $t = 150$ and $t = 600$. The bottom panels display the differences between the GHD prediction and numerical simulations at time $t = 150$ (red) and at time $t = 600$ (green). Number of trials: 3×10^6

In each of the nine cases we have evaluated the Landau-Lifshitz approximations $S_{m,n}^{LL}(\cdot, 1)$, see (51), of the correlators for all $0 \leq n \leq m \leq 2$ using the numerical scheme described in Sect. 4.1.1. Their graphs are displayed in Figs. 1-3 as dashed lines. The correlators $S_{0,0}, S_{1,1}, S_{2,2}, S_{0,2}$ are even in j and $S_{0,1}, S_{1,2}$ are odd, in agreement with (30). In each panel, there is a left and right moving outer peak. At low pressures and high temperatures the scaling

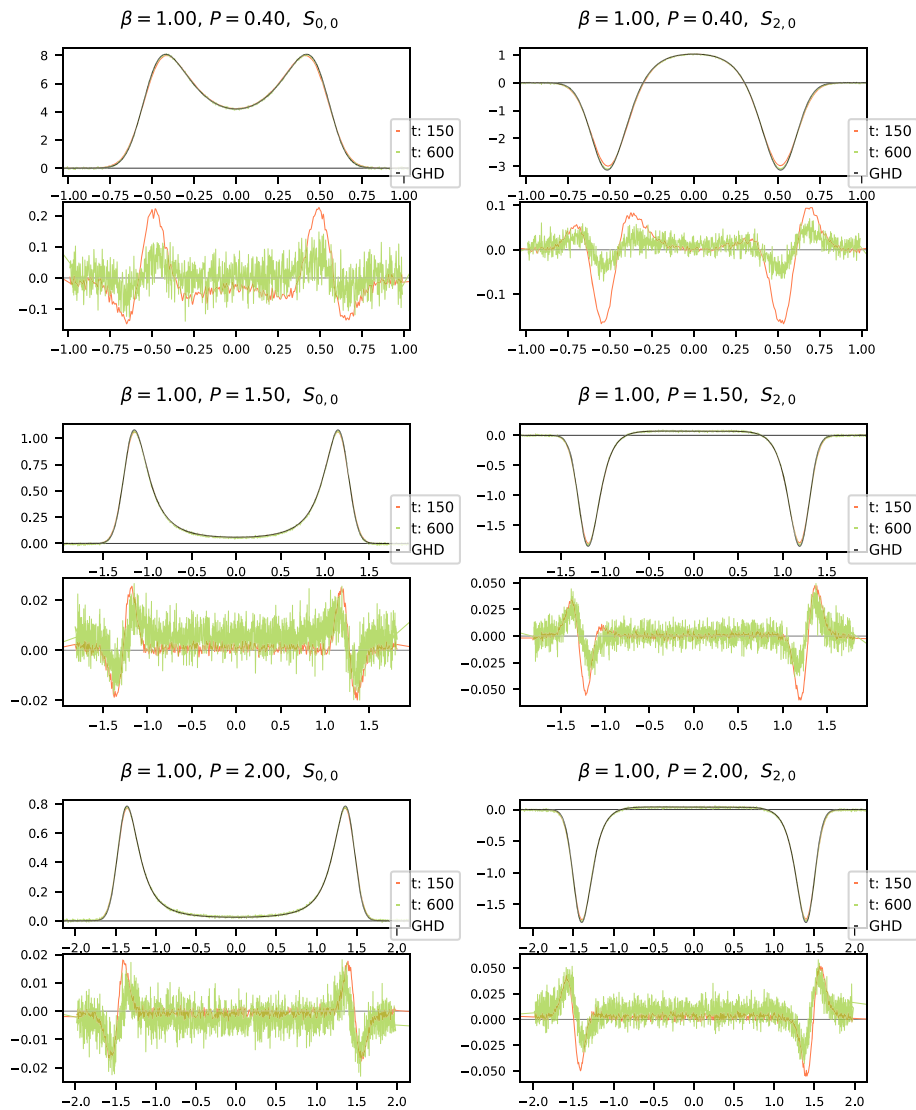


Fig. 5 Toda correlation functions $S_{0,0}$ (left) and $S_{2,0}$ (right) for $\beta = 1$ and increasing pressure (top to bottom). For each value of β and P the top panels show GHD prediction vs. numerical simulations as in Fig. 2 but with the molecular dynamics evaluated at two times $t = 150$ and $t = 600$. The bottom panels display the differences between the GHD prediction and numerical simulations at time $t = 150$ (red) and at time $t = 600$ (green). Number of trials: 3×10^6

function has still a pronounced inner structure. In particular $S_{2,2}$ can have a local maximum at 0. Even further into this regime (not displayed) the diagonal correlators are approximately of the form

$$a_0^2 e^{-\beta w^2/2}, \quad (a_1 w)^2 e^{-\beta w^2/2}, \quad (a_2 w^2 + a_3)^2 e^{-\beta w^2/2} \tag{59}$$

with coefficients a_0, \dots, a_3 depending on P, β . Upon increasing P and β the outer peaks become narrower and move faster. The inner structure reduces to being essentially flat. Such

behavior reflects that in this parameter regime the DOS is proportional to the derivative of the Wigner semicircle law, which is supported by a finite interval.

The colored lines in Figs. 1-3 show our numerical results for the corresponding molecular dynamics. According to the predicted ballistic scaling (52) we plot $tS_{m,n}(j, t)$ as a function of j/t for $t = 600$. Here the values of $S_{m,n}(j, t)$ are approximated using the numerics explained in Sect. 4.1.2.

The agreement between linearized GHD and MD is striking, in particular since there are no adjustable parameters. In all of the 54 comparisons shown in Figs. 1-3 the GHD predictions for the outer peaks and their inner structure are in excellent agreement with the ones observed from molecular dynamics at time $t = 600$. As we show in more detail in the next subsection the largest deviations occur mostly near the outer peaks and do not exceed 3.5% of the peaks' maximal values.

4.3 Deviation of Linearized GHD from MD at Times $t = 150$ and $t = 600$

The purpose of this subsection is twofold. On the one hand, we have a look at the small differences between GHD predictions and molecular dynamics simulations that can hardly be detected in Figs. 1-3. On the other hand, we indicate how these differences evolve in time by including time $t = 150$ for the molecular dynamics. Recall that the GHD predictions are time-invariant in the scaling $y \mapsto tS_{m,n}(yt, t)$ we have chosen, see (52). It would be interesting to investigate the rate of convergence at which the difference tends to 0 as $t \rightarrow \infty$ and whether such a rate exists. As it turned out, the resolution of our numerical experiments is far too weak to say anything meaningful about this question, and we leave it for future research.

From the 54 comparisons that are displayed in Figs. 1-3 we select 12 cases that are representative and show all the phenomena that we have observed. In Fig. 4 we consider correlations $S_{1,1}$ and $S_{1,0}$ at medium pressure (cf. Table 1) for all three values of β . The small scale fluctuations displayed in the bottom panels are due to the approximation of expectation values by empirical averages. Their amplitudes become smaller if one increases the number of trials. Note that the difference in amplitudes of these fluctuations between $t = 150$ and $t = 600$ is mostly due to the scaling $y \mapsto tS_{m,n}(yt, t)$ that we use. This implies that the values of the correlations are multiplied by a factor that is 4 times larger at the later time. The same holds for the plots in Fig. 5 where the correlations $S_{0,0}$ and $S_{2,0}$ are shown for fixed $\beta = 1$ and our three different choices for pressure. We now summarize our main findings:

- (1) The deviations occur mostly near the outer peaks and amount to 1.5%-3.5% of the peaks' maximal values at time $t = 600$.
- (2) There appear to be small but systematic deviations concerning the shapes of the outer peaks in all cases. One would need to conduct experiments with a higher resolution, i.e. more sites and consequently larger times and more trials, to determine whether there is indeed such a systematic deviation. With the resolution present in our experiments, the question of a systematic deviation with respect to the shape of the peak cannot be decided.
- (3) In some of the experiments the maximal deviations would be significantly smaller if a constant only depending on the values of β, P, m, n is added to all values of $S_{m,n}(j, t)$, see e.g. correlations $S_{0,0}$ and $S_{2,0}$ for $\beta = 1, P = 0.4$ in Fig. 5. This seems to be related to the approximation errors for the means $\langle r \rangle, \langle p \rangle$, and $\langle e \rangle$, that appear to be less pronounced in the case of momentum p . We have observed that these deviations decrease as the number

of trials is increased and we do not expect a systematic deviation between GHD and MD in this respect.

- (4) For $(\beta; P) \in \{(0.5; 0.95), (0.5; 1.21)\}$ we observe that the size of the deviations is essentially the same for times $t = 150$ and $t = 600$ whereas for $(\beta; P) \in \{(0.5; 0.32), (1; 0.4), (2; 0.52), (2; 2.55), (2; 3.53)\}$ these deviations are significantly larger at the smaller time. The remaining two cases $(\beta; P) \in \{(1; 1.5), (1; 2)\}$ are somewhat in between, also depending on the correlation function that is considered, see Fig. 5. This is an indication that the speed of convergence of $tS_{m,n}(yt, t)$ to the GHD prediction $S_{m,n}^{LL}(y, 1)$ as $t \rightarrow \infty$ depends on the values of β and P . As a rule we have observed that both increasing temperature or increasing pressure leads to a faster speed of convergence.

5 Further Comments

We list a few observations of interest.

- (1) As can be seen from Table 1, we picked the intermediate pressure such that $\nu \simeq 0$. In the particle picture $\nu = 0$ corresponds to the boundary condition $q_1 = q_N$. In thermal equilibrium, the positions then perform an unbiased random walk with typical excursions of order \sqrt{N} . Thus, the free volume is of order $1/\sqrt{N}$. The particles are extremely dense and the picture of successive pair collisions breaks down completely. So one might wonder whether GHD is still valid under such extreme conditions. $\nu = 0$ poses no particular difficulties for MD simulations. In GHD, the factor $1/\nu$ appears in the expression for v^{eff} , see Eq. (50). This makes the numerical scheme slow and only values close to $\nu = 0$ are accessible. However, the correlator S changes smoothly through $\nu = 0$. As conclusion, GHD covers also this seemingly singular parameter value.
- (2) Simultaneously, A. Kundu [29] posted a somewhat puzzling note. He considers the parameter values $\beta = 1, P = 1$. When cutting the matrices $C_{m,n}$ and $A_{m,n}$ at low orders, the resulting $S_{m,n}$ consists of a few δ -peaks which move at constant velocity. After ballistic scaling, with high precision, they turn out to lie on the profile obtained from GHD. A theoretical explanation seems to be missing.
- (3) In [30] the molecular dynamics of Toda lattice correlations are simulated for the potential

$$V_{\text{kd}}(x) = \frac{g}{\gamma} e^{-\gamma x} \tag{60}$$

with arbitrary $\gamma, g > 0$. To distinguish their parameters from ours, the variables in [30] are here denoted by $\bar{t}, \bar{r}, \bar{P}, \bar{\beta}$. \bar{P} is the physical pressure and, comparing the Gibbs weights, one obtains the relations

$$\beta = \frac{g}{\gamma} \bar{\beta}, \quad P = \frac{1}{\gamma} \bar{P} \bar{\beta}. \tag{61}$$

From the equations of motions one deduces

$$\bar{t} = \frac{1}{\sqrt{\gamma g}} t, \quad r(t) = \gamma \bar{r}(\bar{t}), \quad p(t) = \frac{g}{\gamma} \bar{p}(\bar{t}). \tag{62}$$

Thus, translating to our units, the MD simulations reported in [30] are (a) $P = 0.01, \beta = 0.01, N = 1024, t = 400$, (b) $P = 1, \beta = 1, N = 1024, t = 200, 300$, and (c) $P = 400, \beta = 400, N = 256, t = 80$. In fact, in all three cases the time scales are identical, $t = \bar{t}$. Since GHD was not available yet, no comparison could have been attempted.

Case (a) is a very dilute chain. In this limit $\nu\rho_p$ is a mean zero Gaussian. The dressed functions become polynomials as $\zeta_0^{\text{dr}}(w) = a_0$, $\zeta_1^{\text{dr}}(w) = a_1 w$, and $\zeta_2^{\text{dr}}(w) = a_2 w^2 + a_3$ with coefficients a_0, \dots, a_3 depending on P, β , compare with (59). Note that for a noninteracting fluid a_3 would vanish. As a result $S_{0,0}$ is Gaussian, $S_{1,1}$ has two peaks, and $S_{2,2}$ has either two or three peaks. This is in good agreement with [30] and explains our motivation not to venture into the low pressure regime. Case (b) interpolates between our $\beta = 1, P = 0.40$ and $\beta = 1, P = 1.5$. Note that now $S_{0,0}$ has developed a local minimum at $w = 0$, which is very different from the structure in the dilute regime. On the other hand, $S_{2,2}$ still has a local maximum at $w = 0$, as is the case for low pressure/high temperature.

An interesting parameter value is (c), which requires more detailed studies. The issue is the behavior of the Toda chain at very low temperatures. Simply letting $\beta \rightarrow \infty$ will freeze any motion. But the simultaneous limit $\beta \rightarrow \infty$ with $P = \bar{P}\beta$ at fixed physical pressure \bar{P} is meaningful, at least on the level of the free energy and the Lax density of states. To understand the dynamical behavior, the effective potential is expanded as

$$e^{-r} + \bar{P}r \simeq \frac{1}{2}\bar{P}(r - r_0)^2 + c_0 \quad (63)$$

at its minimum r_0 . Since β is large, the initial fluctuations are of order $1/\sqrt{\beta}$. Therefore the dynamics can be approximated by a harmonic chain with $\omega^2 = \bar{P}$. The equilibrium time correlations of the harmonic chain have intricate oscillatory behavior [22], which in the large β limit should match with the Toda lattice, as partially evidenced by the results in [30]. Clearly, GHD cannot reproduce such fine details. Nevertheless, when averaged on suitable scales, the coarse behavior of spacetime oscillations for the harmonic chain correlations might be visible.

Acknowledgements This material is based upon work supported by the National Science Foundation under Grant No. 1440140, while five of the authors were in residence at the Mathematical Sciences Research Institute in Berkeley, California, during the fall semester of 2021. We thank both reviewers for illuminating comments and suggestions. The authors would like to thank the Isaac Newton Institute for Mathematical Sciences, Cambridge, for support and hospitality during the programme “Dispersive hydrodynamics: mathematics, simulation and experiments, with applications in nonlinear waves” where some work on this paper was undertaken. This work was supported by EPSRC grant no EP/R014604/1. TG acknowledges the support of the European Union’s H2020 Marie Skłodowska–Curie grant No. 778010 *IPaDEGAN*, of INdAM/GNFM and of the research project Mathematical Methods in NonLinear Physics (MMNLP), Gruppo 4-Fisica Teorica of INFN. GM is financed by the KAM grant number 2018.0344. KTRM was supported by a Visiting Wolfson research fellowship from the Royal Society.

Funding Open access funding provided by Royal Institute of Technology.

Open Access This article is licensed under a Creative Commons Attribution 4.0 International License, which permits use, sharing, adaptation, distribution and reproduction in any medium or format, as long as you give appropriate credit to the original author(s) and the source, provide a link to the Creative Commons licence, and indicate if changes were made. The images or other third party material in this article are included in the article’s Creative Commons licence, unless indicated otherwise in a credit line to the material. If material is not included in the article’s Creative Commons licence and your intended use is not permitted by statutory regulation or exceeds the permitted use, you will need to obtain permission directly from the copyright holder. To view a copy of this licence, visit <http://creativecommons.org/licenses/by/4.0/>.



References

1. Allez, R., Bouchaud, J., Guionnet, A.: Invariant β ensembles and the Gauss-Wigner crossover. *Phys. Rev. Lett.* **109**, 1–5 (2012)

2. Bastianello, A., Doyon, B., Watts, G., Yoshimura, T.: Generalized hydrodynamics of classical integrable field theory: the Sinh-Gordon model. *SciPost Phys.* (2018). <https://doi.org/10.21468/SciPostPhys.4.6.045>
3. Beijeren, H.: Exact results for anomalous transport in one-dimensional Hamiltonian systems. *Phys. Rev. Lett.* **108**, 180601 (2012). <https://doi.org/10.1103/PhysRevLett.108.180601>
4. Bertini, B., Collura, M., De Nardis, J., Fagotti, M.: Transport in out-of-equilibrium XXZ chains: exact profiles of charges and currents. *Phys. Rev. Lett.* **117**, 207201 (2016)
5. Bulchandani, V., Vasseur, R., Karrasch, C., Moore, J.: Solvable hydrodynamics of quantum integrable systems. *Phys. Rev. Lett.* **119**, 220604 (2017)
6. Bulchandani, V., Cao, X., Moore, J.: Kinetic theory of quantum and classical Toda lattices. *J. Phys. A: Math. Theor.* **52**, 33LT01 (2019)
7. Castro-Alvaredo, O., Doyon, B., Yoshimura, T.: Emergent hydrodynamics in integrable quantum systems out of equilibrium. *Phys. Rev. X* **6**, 041065 (2016)
8. Das, A., Kulkarni, M., Spohn, H., Dhar, A.: Kardar-Parisi-Zhang scaling for an integrable lattice Landau–Lifshitz spin chain. *Phys. Rev. E* (2019). <https://doi.org/10.1103/PhysRevE.100.042116>
9. Doyon, B.: Exact large-scale correlations in integrable systems out of equilibrium. *SciPost Phys.* (2018). <https://doi.org/10.21468/SciPostPhys.5.5.054>
10. Doyon, B.: Generalized hydrodynamics of the classical Toda system. *J. Math. Phys.* **60**, 073302 (2019)
11. Doyon, B.: Hydrodynamic projections and the emergence of linearised Euler equations in one-dimensional isolated systems. *Comm. Math. Phys.* **391**, 293–356 (2022). <https://doi.org/10.1007/s00220-022-04310-3>
12. Doyon, B., Spohn, H.: Drude weight for the Lieb–Liniger Bose gas. *SciPost Phys.* **3**, 039 (2017). <https://doi.org/10.21468/SciPostPhys.3.6.039>
13. Dupont, M., Moore, J.: Universal spin dynamics in infinite-temperature one-dimensional quantum magnets. *Phys. Rev. B* **101**, 121106 (2020)
14. Fermi, E., Pasta, J. & Ulam, S. Studies of nonlinear problems. (Los Alamos National Laboratory, 1955)
15. Flaschka, H.: The Toda lattice. I. Existence of integrals. *Phys. Rev. B* **3**(9), 1924–1925 (1974)
16. Forrester, P., Mazzuca, G.: The classical β -ensembles with β proportional to $1/N$: from loop equations to Dyson’s disordered chain. *J. Math. Phys.* **62**, 073505 (2021)
17. Forster, D. Hydrodynamic fluctuations, broken symmetry, and correlation functions (1975). <https://inis.iaea.org/search/search.aspx?orig>
18. Gallavotti, G., Miracle-Sole, S.: Absence of phase transitions in hard-core one-dimensional systems with long-range interactions. *J. Math. Phys.* **11**, 147–154 (1970). <https://doi.org/10.1063/1.1665040>
19. Grava, T., Mazzuca, G.: Generalized Gibbs ensemble of the Ablowitz–Ladik lattice, circular β -ensemble and double confluent Heun equation. *Comm. Math. Phys.* **399**, 1689–1729 (2023)
20. Grava, T., Maspero, A., Mazzuca, G., Ponso, A.: Adiabatic invariants for the FPUT and Toda chain in the thermodynamic limit. *Comm. Math. Phys.* **380**, 811–851 (2020)
21. Grava, T., Kriecherbauer, T., Mazzuca, G., McLaughlin, K.: Correlation functions for a chain of short range oscillators. *J. Stat. Phys.* **183**, 1 (2021)
22. Grava, T., Kriecherbauer, T., Mazzuca, G., McLaughlin, K.: Correlation functions for a chain of short range oscillators. *J. Stat. Phys.* **183**, 1–31 (2021)
23. Guionnet, A., Memin, R.: Large deviations for Gibbs ensembles of the classical Toda chain. *Electron. J. Probab.* **27**, 1–29 (2022)
24. Hairer, E.: Symplectic Integration of Hamiltonian Systems. In: Hairer, E., Wanner, G., Lubich, C. (eds.) *Geometric Numerical Integration: Structure-Preserving Algorithms For Ordinary Differential Equations*, pp. 179–236. Springer, Berlin (2006)
25. Harris, C., Millman, K., Walt, S., Gommers, R., Virtanen, P., Cournapeau, D., Wieser, E., Taylor, J., Berg, S., Smith, N., Kern, R., Picus, M., Hoyer, S., Kerkwijk, M., Brett, M., Haldane, A., Río, J., Wiebe, M., Peterson, P., Gérard-Marchant, P., Sheppard, K., Reddy, T., Weckesser, W., Abbasi, H., Gohlke, C., Oliphant, T.: Array programming with NumPy. *Nature* **585**, 357–362 (2020)
26. Hunter, J.: Matplotlib: a 2D graphics environment. *Comput. Sci. Eng.* **9**, 90–95 (2007)
27. Ilievski, E., Nardis, J., Medenjak, M., Prosen, T.: Superdiffusion in one-dimensional quantum lattice models. *Phys. Rev. Lett.* (2018). <https://doi.org/10.1103/PhysRevLett.121.230602>
28. Kardar, M., Parisi, G., Zhang, Y.: Dynamic scaling of growing interfaces. *Phys. Rev. Lett.* **56**, 889–892 (1986)
29. Kundu, A.: Integrable hydrodynamics of Toda chain: case of small systems. *Euro. Phys. J. Special Topics* **24**, 1–10 (2022). <https://doi.org/10.1140/epjs/s11734-023-00848-y>
30. Kundu, A., Dhar, A.: Equilibrium dynamical correlations in the Toda chain and other integrable models. *Phys. Rev. E* **94**, 062130 (2016)
31. Lam, S., Pitrou, A. & Seibert, S. Numba: A LLVM-based Python JIT compiler. *Proceedings Of The Second Workshop On The LLVM Compiler Infrastructure In HPC.* (2015)

32. Landau, L., Lifshitz, E.: Fluid mechanics, vol. 6. Elsevier, Amsterdam (2013)
33. Lebowitz, J., Percus, J., Sykes, J.: Time evolution of the total distribution function of a one-dimensional system of hard rods. *Phys. Rev.* **171**, 224–235 (1968). <https://doi.org/10.1103/PhysRev.171.224>
34. Ljubotina, M., Žnidarič, M., Prosen, T.: Kardar-Parisi-Zhang physics in the quantum Heisenberg magnet. *Phys. Rev. Lett.* (2019). <https://doi.org/10.1103/PhysRevLett.122.210602>
35. Manakov, S.: Complete integrability and stochastization of discrete dynamical systems. *Ž. Èksper. Teoret. Fiz.* **67**, 543–555 (1974)
36. Mazzuca, G. & Memin, R. CLT for β ensembles at high-temperature, and for integrable systems: a transfer operator approach (2023). [arXiv:2304.10323](https://arxiv.org/abs/2304.10323)
37. Mazzuca, G. Toda correlation functions (GitHub, 2022). <https://github.com/gmazzuca/TodaCorrelation>. <https://doi.org/10.1140/epjs/s11734-023-00848-y>
38. Mazzuca, G.: On the mean density of states of some matrices related to the beta ensembles and an application to the Toda lattice. *J. Math. Phys.* **63**, 043501 (2022)
39. Mazzuca, G.: On the mean density of states of some matrices related to the beta ensembles and an application to the Toda lattice. *J. Math. Phys.* **63**, 043501 (2022). <https://doi.org/10.1063/5.0076539>
40. Mazzuca, G., Memin, R.: Large deviations for Ablowitz-Ladik lattice, and the Schur flow. *Electron. J. Probab.* (2023). <https://doi.org/10.1214/23-ejp941>
41. Mendl, C., Spohn, H.: Equilibrium time-correlation functions for one-dimensional hard-point systems. *Phys. Rev. E* **90**, 012147 (2014)
42. Mendl, C., Spohn, H.: Low temperature dynamics of the one-dimensional discrete nonlinear Schrödinger equation. *J. Stat. Mech.: Theory Exp.* **2015**, P08028 (2015)
43. Mendl, C., Spohn, H.: High-low pressure domain wall for the classical Toda lattice. *SciPost Phys. Core.* **5**, 002 (2022)
44. Möller, F., Perfetto, G., Doyon, B., Schmiedmayer, J.: Euler-scale dynamical correlations in integrable systems with fluid motion. *SciPost Phys. Core* (2020). <https://doi.org/10.21468/SciPostPhysCore.3.2.016>
45. Opper, M.: Analytical solution of the classical Bethe ansatz equation for the Toda chain. *Phys. Lett. A* **112**, 201–203 (1985)
46. Schneider, T.: Classical statistical mechanics of lattice dynamic model systems: transfer integral and molecular-dynamics studies. In: Benedek, G., Bilz, H., Zeyher, R. (eds.) *Statics And Dynamics Of Nonlinear Systems*, pp. 212–241. Springer, Berlin (1983)
47. Schneider, T., Stoll, E.: Excitation spectrum of the Toda lattice: a molecular-dynamics study. *Phys. Rev. Lett.* **45**, 997–1002 (1980)
48. Spohn, H. Hydrodynamic scales of integrable many-particle systems (2023). [arXiv:2301.08504](https://arxiv.org/abs/2301.08504)
49. Spohn, H. The Kardar-Parisi-Zhang equation: a statistical physics perspective. *Stochastic processes and random matrices: lecture notes of the Les Houches Summer School July 2015.* **104** pp. 177–227 (2017)
50. Spohn, H.: Nonlinear fluctuating hydrodynamics for anharmonic chains. *J. Stat. Phys.* **154**, 1191–1227 (2014)
51. Spohn, H.: Ballistic space-time correlators of the classical Toda lattice. *J. Phys. A* **53**, 265004–2650017 (2020)
52. Spohn, H.: Generalized Gibbs ensembles of the classical Toda chain. *J. Stat. Phys.* **180**, 4–22 (2020)
53. Spohn, H.: Collision rate ansatz for the classical Toda lattice. *Phys. Rev. E* **101**, 060103(R) (2020)
54. Toda, M.: Vibration of a chain with nonlinear interaction. *J. Phys. Soc. Jpn.* **22**, 431–436 (1967)
55. Toda, M.: *Theory of Nonlinear Lattices*. Springer, Berlin (1989). <https://doi.org/10.1007/978-3-642-83219-2>
56. Yoshimura, T., Spohn, H.: Collision rate ansatz for quantum integrable systems. *SciPost Phys.* **9**, 040 (2020)

Authors and Affiliations

Guido Mazzuca¹  · Tamara Grava^{2,3,4} · Thomas Kriecherbauer⁵ ·
Kenneth T.-R. McLaughlin⁶ · Christian B. Mendl⁷ · Herbert Spohn⁸ 

Tamara Grava
grava@sissa.it

Thomas Kriecherbauer
thomas.kriecherbauer@uni-bayreuth.de

Kenneth T.-R. McLaughlin
kmclaughlin@tulane.edu

Christian B. Mendl
christian.mendl@tum.de

Herbert Spohn
spohn@ma.tum.de

¹ Mathematics, The Royal Institute of Technology, Lindstedtsvägen 25, 114 28 Stockholm, Sweden

² School of Mathematics, University of Bristol, Fry Building, Bristol BS8 1UG, UK

³ Mathematics Area, SISSA, Via Bonomea 265, 34136 Trieste, Italy

⁴ INFN sezione di Trieste, Trieste, Italy

⁵ Mathematics, Universität Bayreuth, Universitätsstraße 30, 95447 Bayreuth, Germany

⁶ Mathematics, Tulane University, 6823 St Charles Ave, New Orleans, LA 70118, USA

⁷ Informatics, Technische Universität München, Boltzmannstraße 3, 85748 Garching, Germany

⁸ Mathematics and Physics, Technische Universität München, Boltzmannstraße 3, 85748 Garching, Germany